



# Improving time-domain prediction of vortex-induced vibration of marine risers

Boyang Zhang<sup>1</sup> · Wei Qiu<sup>1</sup>

Received: 5 July 2017 / Accepted: 13 November 2017 / Published online: 27 November 2017  
© Sociedade Brasileira de Engenharia Naval 2017

## Abstract

The prediction of the vortex-induced vibration (VIV) of marine risers becomes a critical issue as the offshore exploration and production moving into deepwater and ultra-deepwater regions. In this paper, a time-domain model, based on a forcing algorithm and on high Reynolds number experimental data, was further developed to predict the VIV of rigid and flexible risers. The forcing algorithm was integrated into a global-coordinate-based finite-element program. At each time step, the hydrodynamic forces on a riser, including added mass, lift and drag forces, were calculated for each element based on two non-dimensional state variables—the amplitude ratio and the reduced velocity. The state variables were determined from a zero up-crossing analysis of the time history of the cross-flow displacement. Validation studies were carried out for a full-scale rigid riser segment in a uniform flow and a flexible riser in a stepped current. The predicted motions of the risers were compared with experimental data and the motions predicted by other numerical models.

**Keywords** Marine risers · Vortex-induced vibration · Time domain · Finite element method

## List of symbols

$A$	Amplitude of vibration
$A_z$	Cross-flow motion amplitude
$A^*$	Cross-flow amplitude ratio
$C_d$	In-line drag coefficient
$C_{d0}$	Mean in-line drag coefficient
$C_{lv}$	Cross-flow lift coefficient
$C_m$	Added mass coefficient
$D$	Diameter of the cylinder
$f_{nw}$	Natural frequency in still water
$f_{osc}$	Oscillation frequency
$F_D$	In-line drag force amplitude
$F_{D0}$	Mean in-line drag force
$F_L$	Cross-flow lift force amplitude
$F_x$	Total in-line drag force
$F_z$	Total cross-flow lift force
$F_{\dot{z}}$	Cross-flow lift force in phase with velocity
$F_{\ddot{z}}$	Cross-flow lift force in phase with acceleration
$L$	Length of the cylinder
$m$	Mass of the cylinder

$m'$	Added mass of the cylinder
$k$	Spring stiffness
$k_x$	Structural stiffness in the in-line direction
$k_z$	Structural stiffness in the cross-flow direction
$t$	Time
$T_{app}$	Apparent period of motion
$U$	Incoming flow velocity
$U^*$	Nominal reduced velocity
$V$	Relative normal velocity between the incoming flow and the structure
$V_r$	Reduced velocity
$V_{tow}$	Towing speed of carriage
$Z_{max}$	Maximum transverse displacement in a motion cycle
$Z_{min}$	Minimum transverse displacement in a motion cycle
$\rho$	Density of fluid

## 1 Introduction

Marine risers subjected to ocean currents can experience fluctuating forces caused by asymmetric vortex shedding. These forces can be decomposed into drag forces in-line with the flow direction and lift forces in the cross-flow direction. The oscillating forces may result in non-linear

✉ Wei Qiu  
qiuw@mun.ca

<sup>1</sup> Advanced Marine Hydrodynamics Laboratory, Department of Ocean and Naval Architectural Engineering, Memorial University, St. John's, Canada

and near-periodic vibrations, i.e., vortex-induced vibration (VIV). VIV can lead to a reduced fatigue life of a marine riser. If the vortex-shedding frequency is in the proximity of one of the riser's natural frequencies, the riser will vibrate at an amplitude comparable to the riser diameter. This phenomenon is known as lock-in, which is more difficult to be predicted when the riser operates in the deepwater and ultra-deepwater environments, where the incoming current varies both spatially and temporally along the riser span.

Many experiments have been carried out to investigate VIV of marine risers. Due to the large length-to-diameter ratios of risers, most of tests were conducted on a segment of a riser in full scale or in model scale due to facility limitations. Field experiments on full-scale risers are relatively rare due to many factors such as environmental conditions and challenges in sensor installation and data acquisition.

Extensive studies have been performed on VIV prediction based on the frequency-domain methods. Semi-empirical frequency-domain methods, such as SHEAR7, VIVA [1] and VIVANA [2], are widely used in the offshore industry. The modal analysis was employed in these models to determine the modes likely subject to VIV and the corresponding natural frequencies. For each mode, the reduced velocity is calculated based on frequency and flow information. An excitation or damping force is then applied according to the reduced velocity. Figure 1 presents a typical damping model used in SHEAR7 [3] where the damping is only defined for reduced velocities lower than 5 and greater than 8. For reduced velocities between 5 and 8, excitation was assumed to occur and a separate model was implemented.

There are limitations in the frequency-domain models. For example, they are inadequate to deal with non-linearities such as temporally and spatially varying currents, dynamic

boundary conditions and the coupled in-line and cross-flow VIV. Furthermore, both positive and negative lift coefficients exist in the lock-in region, as shown in the work of Gopalkrishnan [4] and Oakley and Spencer [5]. This indicates that hydrodynamic excitation and damping may not be independently considered.

To address the limitations in the frequency-domain methods, time-domain approaches have been developed in recent years. For example, Lie [6] developed a finite element model in the time domain to simulate the transverse VIV of a flexible cylinder in a shear flow. The lift forces were approximated by two components, one at the cylinder motion frequency and one at the Strouhal frequency for a stationary cylinder. The cylinder frequency force was obtained from the experimental results of a cylinder with forced harmonic motions. The latter component was assumed to be less important than the cylinder frequency component and was modeled as a sinusoidal lift force by using the lift coefficient from the experimental data for a stationary cylinder.

Finn et al. [7] developed a time-domain procedure for VIV prediction. The cross-flow lift force was calculated using a time-dependent lift coefficient. The frequency and the phase of the lift coefficient were determined using an empirical method. In this method, a lock-in decision tree was developed to identify the flow–riser interaction situation and to determine the corresponding lift coefficient by using three non-dimensional parameters, i.e., the ratio of the VIV amplitude to the riser diameter, the ratio of the natural frequency of a particular mode to the shedding frequency, and the ratio of transverse vibration frequency to the shedding frequency. The riser responses were computed with a finite element program, ABAQUS, and a user subroutine in ABAQUS was developed to calculate hydrodynamic forces using riser displacements, velocities and accelerations.

Based on the algorithm of Finn et al. [7] for cross-flow VIV prediction, Sidarta et al. [8] added the computation of in-line VIV forces in SimVIV to account for both cross-flow and in-line VIV analysis. In their work, the in-line vortex shedding frequency was two times that of the cross-flow VIV and the added mass coefficient was assumed as 1.0. Thorsen et al. [9] proposed a time-domain model for cross-flow VIV simulation. In their work, the synchronization between the lift force and the structural motion was considered to have positive energy transfer from fluid to cylinder.

In this study, a time-domain VIV prediction model was further developed based on the work of Spencer et al. [10] and Ma et al. [11]. The forcing algorithm was improved by using the zero up-crossing analysis of the time-history of the cross-flow displacement, which was applied to determine two state variables, the amplitude ratio and the reduced velocity. The state variables were then employed to obtain the hydrodynamic coefficients by interpolating a high Reynolds number database from the forced oscillation tests [5]

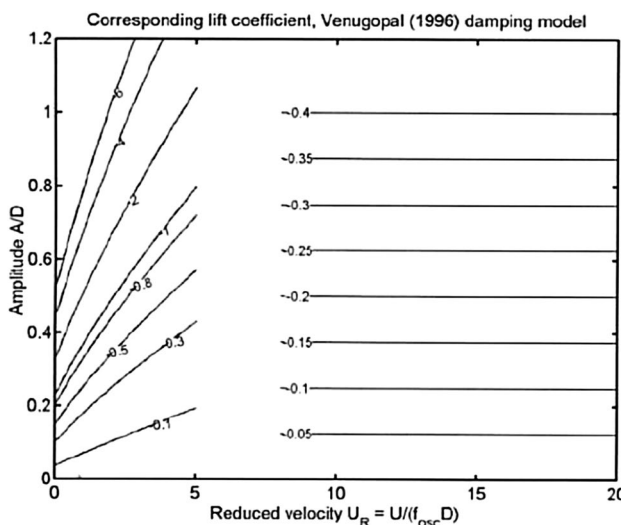


**Fig. 1** Venugopal's damping model for low and high  $V_r$  [3]

in the DeepStar Joint Industry Project (JIP). This improved forcing algorithm was integrated into a global-coordinate-based finite element program, MAPS-Mooring, to predict VIV in the time domain. Validation studies were carried out for a segment of full-scale riser undergoing free VIV in a uniform flow and a flexible riser in a stepped current. The numerical predictions were compared with the experimental results and those by other numerical models.

## 2 High Reynolds number VIV tests and hydrodynamic database

Both forced and free vibration tests were conducted on a full-scale rigid riser segment with a diameter of 0.325 m and a length of 6.02 m in the DeepStar JIP [5]. In the forced VIV tests, the cylinder was towed horizontally through water with prescribed oscillations in the transverse direction. End plates were fitted at both ends to minimize the 3-D flow effect. Reynolds numbers were from  $10^5$  to over  $10^6$ .

The measured hydrodynamic forces exerting on the cylinder were decomposed into the in-line drag force and the cross-flow lift force. The lift force was further decomposed into one component in phase with the velocity and one in phase with acceleration. The non-dimensional hydrodynamic coefficients, including the lift coefficient  $C_{lv}$ , the added mass coefficient  $C_m$ , and the in-line drag coefficient  $C_d$ , were then obtained as follows according to the work of Oakley and Spencer [5]:

$$\begin{aligned} C_{lv} &= \frac{F_z \cdot \dot{z}}{\frac{1}{2}\rho D L V_{\text{tow}}^2 \cdot \frac{1}{\sqrt{2}}\sigma_z} \\ C_m &= \frac{-F_z \cdot \ddot{z}}{\frac{\pi}{4}\rho D^2 L \cdot \sigma_z^2} \\ C_d &= \frac{F_x \cdot \dot{z}}{\frac{1}{2}\rho D L V_{\text{tow}}^2 \cdot \frac{1}{\sqrt{2}}\sigma_z}, \end{aligned} \quad (1)$$

where  $D$  is the diameter,  $L$  is the segment length,  $\rho$  is the fluid density,  $V_{\text{tow}}$  is the constant towing speed,  $z$  is the cross-flow displacement, the overdots denote the differentiation with respect to time,  $F_z$  is the lift force,  $F_x$  is the in-line drag force, and  $\sigma$  represents the root-mean-square (RMS) value.

These non-dimensional hydrodynamic coefficients were presented in the database in terms of the amplitude-to-diameter ratio,  $A^*$ , and the reduced velocity,  $V_r$ , which are defined as:

$$\begin{aligned} A^* &= \frac{A}{D} \\ V_r &= \frac{V_{\text{tow}}}{f_{\text{osc}} D}, \end{aligned} \quad (2)$$

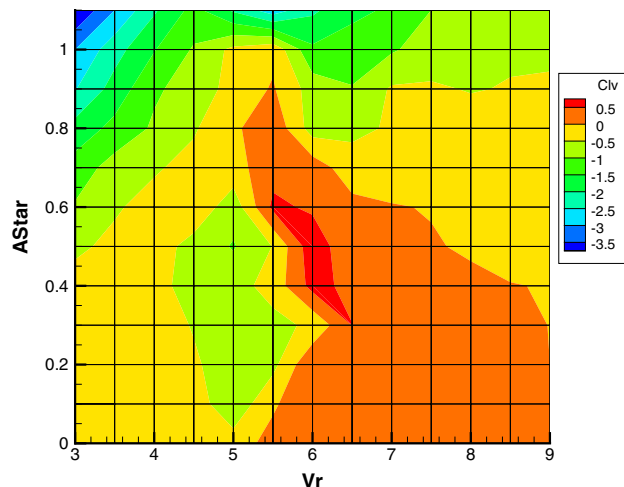


**Fig. 2** 2-D lift coefficients in terms of ( $A^*$ ,  $V_r$ )

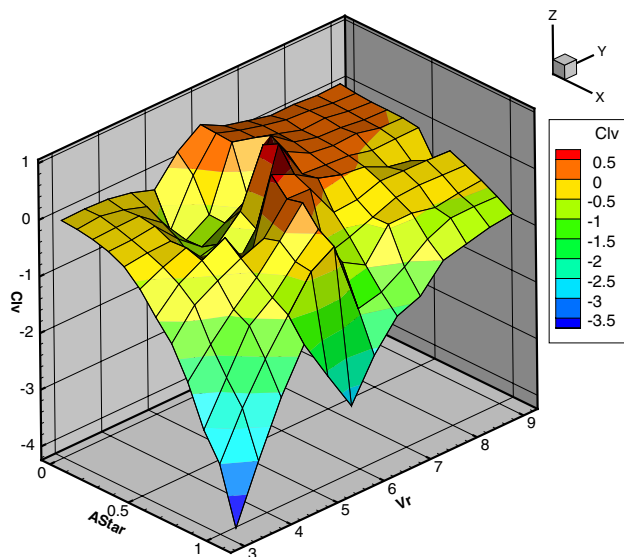


**Fig. 3** 3-D contours of lift coefficients in terms of ( $A^*$ ,  $V_r$ )

where  $f_{\text{osc}}$  is the forced oscillation frequency,  $A$  is the motion amplitude.

Figures 2 and 3 present the 2-D and 3-D contours of  $C_{lv}$ , respectively, for a bare rough cylinder [5]. It should be noted that both positive and negative values of  $C_{lv}$  exist in the range of  $5 < V_r < 8$ . When  $C_{lv}$  is positive, energy is input into the cylinder and the VIV motion is excited. When  $C_{lv}$  is negative, energy is extracted from the structure and the VIV motion is damped.

The added mass coefficients,  $C_m$ , can also be positive or negative. The in-line drag force oscillates around a mean value at a frequency twice that of the lift force. The drag coefficients,  $C_d$ , include a mean part and an oscillating

component. These coefficients are presented in Figs. 4 and 5. The database including these hydrodynamic coefficients was used in the present forcing algorithm.

### 3 Numerical formulations

#### 3.1 Time-domain VIV prediction model

Based on the work of Spencer et al. [10] and Ma et al. [11], the hydrodynamic forces on a cylinder in the current VIV cycle were calculated in terms of the hydrodynamic coefficients,  $C_{lv}$ ,  $C_m$  and  $C_d$ , which were interpolated from the database by utilizing the state variables,  $A^*$  and  $V_r$ , determined from the last cycle. The underlining assumption was that the fluid has no memory of what happened prior. Note that the state variables were calculated by a zero up-crossing analysis of the cross-flow velocity in the work of Spencer et al. [10] and Ma et al. [11].

In the present model, the zero up-crossing analysis was applied to the cross-flow displacement considering there may be more than one frequency components in the time series of cross-flow velocity. As shown in Fig. 6, the maximum and minimum displacements,  $Z_{\max}$  and  $Z_{\min}$ , as well as the apparent period,  $T_{\text{app}}$ , are identified in a cycle and used to calculate the current state variables,  $A^*$  and  $V_r$ , as below:

$$\begin{aligned} A^* &= \frac{Z_{\max} - Z_{\min}}{2D} \\ V_r &= \frac{V T_{\text{app}}}{D}. \end{aligned} \quad (3)$$

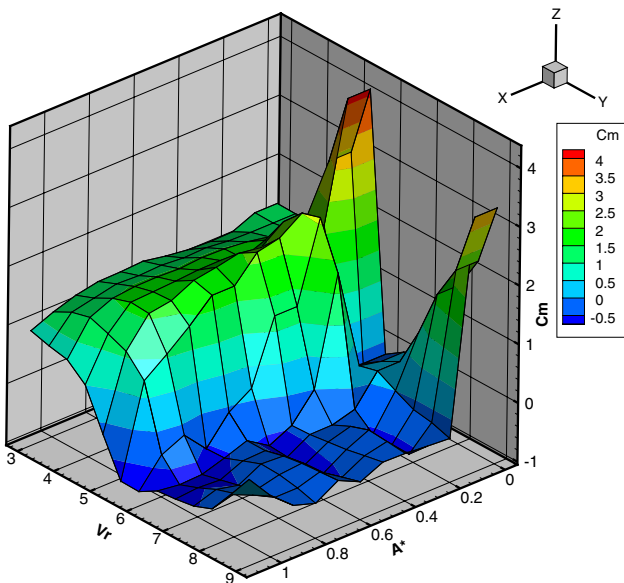


**Fig. 4** Added mass coefficients in terms of ( $A^*$ ,  $V_r$ )

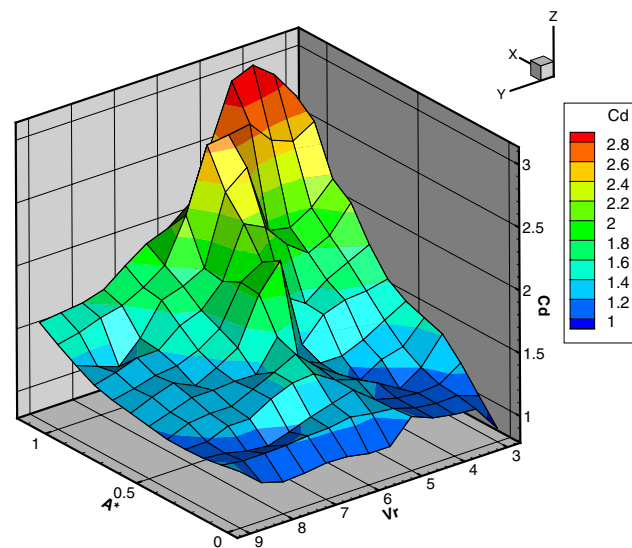


**Fig. 5** Drag coefficients in terms of ( $A^*$ ,  $V_r$ )

The equation of motion for a typical one-degree-of-freedom (1-DOF) mass-spring-damper system is:

$$m\ddot{z} + c\dot{z} + kz = F_z(t), \quad (4)$$

where  $m$  is the mass,  $c$  is the structural damping coefficient,  $k$  is the spring stiffness, and  $F_z(t)$  is the external force varied with time  $t$ .

Assuming  $z(t) = A_z \sin(\omega t)$  is a steady-state solution of Eq. (4), the corresponding velocity and acceleration are  $\dot{z} = \omega A_z \cos(\omega t)$  and  $\ddot{z} = -\omega^2 A_z \sin(\omega t)$ , respectively, where  $A_z$  and  $\omega$  are the amplitude and the angular frequency of the motion, respectively. The overdots denote the differentiation with respect to time.

In an 1-DOF VIV, it is assumed that the angular frequency of the transverse lift force,  $F_z(t)$ , is equal to that of

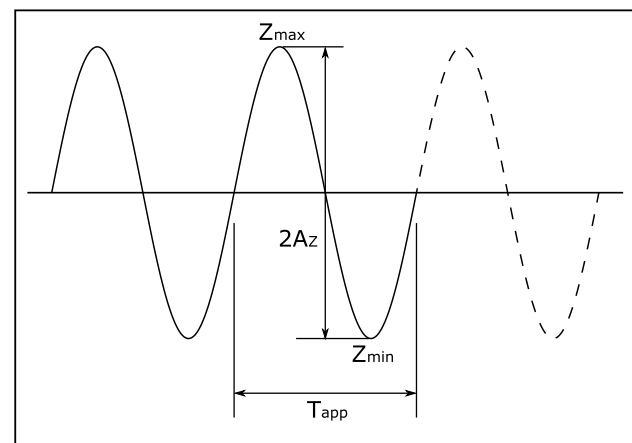


**Fig. 6** Zero up-crossing analysis of displacement

the transverse motion.  $F_z(t)$  can be decomposed into one component in phase with velocity,  $F_{\dot{z}}(t)$ , and one in phase with acceleration,  $F_{\ddot{z}}(t)$ , i.e.,  $F_z(t) = F_{\dot{z}}(t) + F_{\ddot{z}}(t)$ . According to the data reduction procedure as shown in Eq. (1),  $F_{\dot{z}}(t)$  and  $F_{\ddot{z}}(t)$  can be expressed as:

$$\begin{aligned} F_{\dot{z}}(t) &= C_{lv} \cdot \frac{1}{2} \rho D L V^2 \cdot \cos(\omega t) \\ F_{\ddot{z}}(t) &= C_m \cdot \frac{\pi}{4} \rho D^2 L \cdot [-\omega^2 A_z \sin(\omega t)], \end{aligned} \quad (5)$$

where  $V$  is the relative normal velocity between the incoming flow and the oscillating riser.

Moving  $F_{\ddot{z}}(t)$  to the left-hand-side (LHS) of Eq. (4) led to:

$$(m + m')\ddot{z} + c\dot{z} + kz = F_{\dot{z}}(t), \quad (6)$$

where  $m' = C_m \cdot \frac{\pi}{4} \rho D^2 L$  is the added mass.

Assuming the structural damping is small in comparison with the hydrodynamic damping, the structural damping term,  $c\dot{z}$ , in Eq. (4) was therefore neglected in the present model. Note that the hydrodynamic excitation and damping are considered based on the sign of  $C_{lv}$  interpolated from the database.

By substituting Eq. (5) into Eq. (6) and neglecting the structural damping term,  $c\dot{z}$ , the equation of motion in the cross-flow direction is given as:

$$\begin{aligned} [m + m'(A^*, V_r)]\ddot{z} + k_z z \\ = F_L(A^*, V_r) \cos[\omega(t - t_0)], \end{aligned} \quad (7)$$

where  $m'(A^*, V_r)$  is the added mass in the cross-flow direction in terms of  $A^*$  and  $V_r$ ,  $k_z$  is the structural stiffness in the cross-flow direction,  $F_L$  is the lift force amplitude,  $t_0$  is the time instant when the last VIV cycle ends, and

$$\begin{aligned} \omega &= \frac{2\pi}{T_{app}} \\ F_L(A^*, V_r) &= C_{lv}(A^*, V_r) \cdot \frac{1}{2} \rho D L V^2 \\ m'(A^*, V_r) &= C_m(A^*, V_r) \cdot \frac{\pi}{4} \rho D^2 L. \end{aligned} \quad (8)$$

By assuming that the added mass coefficient in the in-line direction equals that in the cross-flow direction, the equation of motion in the in-line direction is described as:

$$\begin{aligned} [m + m'(A^*, V_r)]\ddot{x} + k_x x \\ = F_{D0} + [F_D(A^*, V_r) - F_{D0}] \cos[2\omega(t - t_0)], \end{aligned} \quad (9)$$

where  $x$  is the in-line displacement,  $\ddot{x}$  is the in-line acceleration,  $k_x$  is the structural stiffness in the in-line direction,  $F_{D0}$  is the mean drag force,  $F_D$  is the drag force amplitude, and

$$\begin{aligned} F_{D0} &= C_{d0} \cdot \frac{1}{2} \rho D L V^2 \\ F_D(A^*, V_r) &= C_d(A^*, V_r) \cdot \frac{1}{2} \rho D L V^2, \end{aligned} \quad (10)$$

where  $C_{d0} = 1.0$  is the mean drag coefficient used in this study. Note that the in-line drag force oscillates at a frequency twice that of the cross-flow lift force.

Note that the lift component in phase with velocity and the added mass were both put on the RHS of the equation of motion in the work of Spencer et al. [10] and Ma et al. [11].

As for the initial conditions, the initial hydrodynamic coefficients were set as  $C_{m0} = 1.0$  and  $C_{lv0} = 1.0$  in the first cycle. Since the non-dimensional vortex-shedding frequency is approximately 0.18 over a large range of the sub-critical Reynolds number regime, the initial forcing frequency was set according to  $\omega = \frac{2\pi V}{V_r D}$  with  $V_r = 5.5$ . The initial displacement and velocity in the VIV simulations were set as their static equilibrium values.

The hydrodynamic coefficients used in the time-domain simulations were interpolated from the scattered data points in the database. The SURF routine from the IMSL Numerical Library was employed by Spencer et al. [10] for interpolation. However, this approach does not lead to accurate interpolation near the boundaries of the data set or a region with steep changes in the slope of data surface. Ma et al. [11] improved the interpolation by using a bi-linear scheme.

The effects of surface interpolation algorithms on the time-domain VIV prediction model was further investigated in this work using bi-cubic and Non-Uniform Rational B-Spline (NURBS) surface interpolations. No significant improvement was found when using higher-order methods. In addition, the higher-order interpolation would lead to inaccuracy at some data points. Therefore, a bilinear interpolation approach equivalent to that by Ma et al. [11] was adopted in this study.

### 3.2 Finite element analysis

The improved forcing algorithm was integrated into a global-coordinate-based finite-element program, MAPS-Mooring [12], an in-house program developed according to the work of Garrett [13], for static and dynamic structural analysis of mooring lines and risers. A summary of the program can be found in the work of Ma et al. [11]. It should be pointed out that no assumption was made on the correlation length in the forcing algorithm. The correlation between neighboring elements was automatically considered through structural responses.

In the present studies, different time integration schemes, other than the first-order Adams–Moulton method in MAPS-Mooring, were investigated for finite element analysis. It

**Table 1** Parameters and test conditions in the free VIV tests

Item	Value
Water depth (m)	7.00
Diameter (m)	0.325
Total length (m)	6.02
Total mass (kg)	800
Mass ratio	1.56
Spring stiffness (kN/m)	40
Boundary conditions	Both ends spring-supported

was indicated that these methods did not lead to significant improvements in the predictions. The original numerical method used in MAPS-Mooring was then adopted.

In the work of Ma et al. [11], uniform hydrodynamic forces were applied on each element which were determined from the state variables by using the velocity of the second node of a finite element. In the present computations, hydrodynamic forces were applied on two nodes of each element (i.e., linear load distribution). The state variables at the two end nodes of each element were determined from the zero up-crossing analysis of the nodal displacements. This results in a more continuous hydrodynamic force distribution along the riser span. Note that the global maximum and minimum nodal displacements were used in the work of Ma et al. [11] to obtain state variables and the local motion characteristics were analyzed for each element.

## 4 Validation studies

### 4.1 1-DOF VIV of a rigid riser

The time-domain VIV prediction algorithm was first validated by applying it to the 1-DOF free VIV of the rigid cylinder which was used in the DeepStar JIP to generate the hydrodynamic database. The cylinder was elastically connected to springs with an overall stiffness of 40 kN/m and towed at various constant speeds in a towing tank. The particulars of the riser segment and test conditions are given in Table 1.

The initial condition for the simulations was set as when the riser was in the static equilibrium. In the simulations, one element was used and the time step was set as 0.005 s. The towing velocities were from 0.8 to 2.8 m/s. The time series of the non-dimensional transverse motion under these velocities are presented in Figs. 7, 8, 9, 10, 11 and 12 in terms of nominal reduced velocities which are defined as:

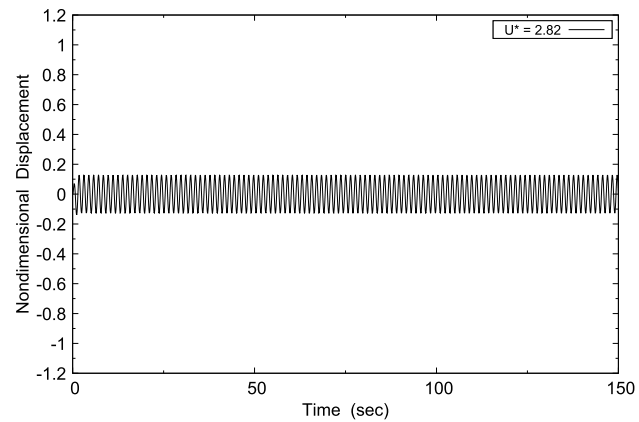


**Fig. 7** Rigid riser 1-DOF VIV under velocity of 0.8 m/s

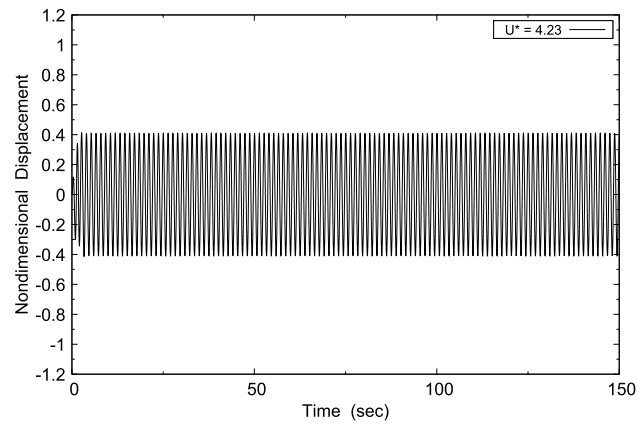


**Fig. 8** Rigid riser 1-DOF VIV under velocity of 1.2 m/s

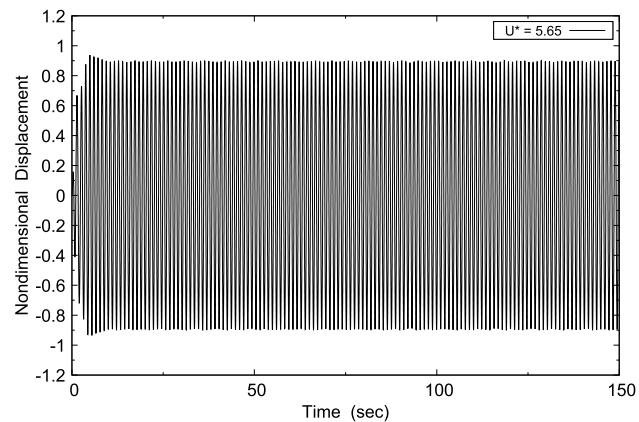


**Fig. 9** Rigid riser 1-DOF VIV under velocity of 1.6 m/s

$$U^* = \frac{U}{f_{\text{nw}} D}, \quad (11)$$

where  $U$  is the incoming flow velocity,  $f_{\text{nw}}$  is the natural frequency in still water, and  $D$  is the diameter of the riser.

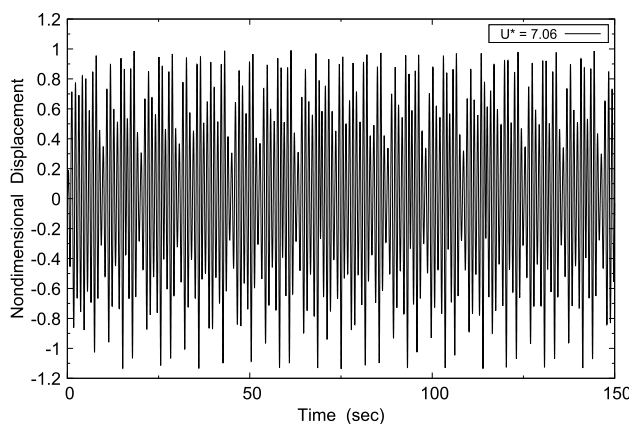


**Fig. 10** Rigid riser 1-DOF VIV under velocity of 2.0 m/s

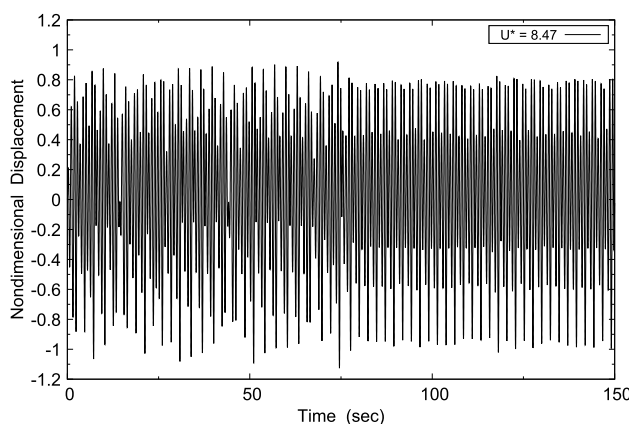


**Fig. 11** Rigid riser 1-DOF VIV under velocity of 2.4 m/s

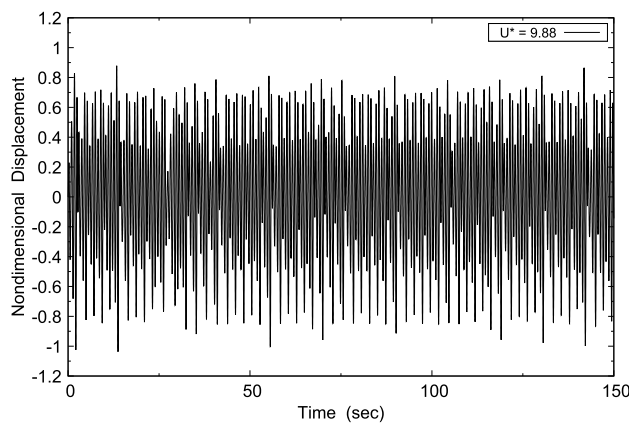


**Fig. 12** Rigid riser 1-DOF VIV under velocity of 2.8 m/s

As shown in Figs. 7, 8 and 9, the VIV responses at the towing velocities of 0.8, 1.2 and 1.6 m/s reach steady state shortly after the initial conditions.

As the nominal reduced velocity was increased, beat patterns are shown in the time series of motion in Figs. 10,

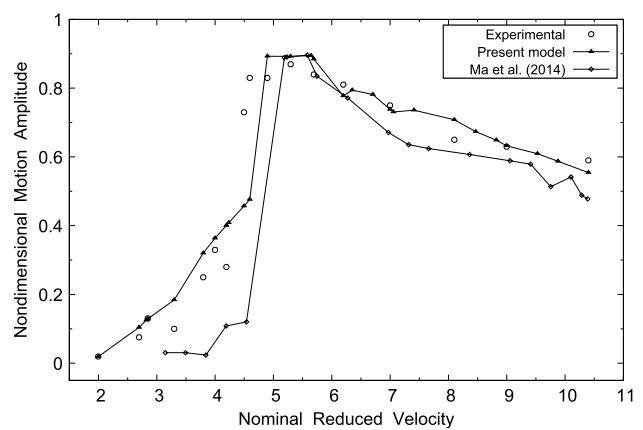


**Fig. 13** Rigid riser 1-DOF VIV amplitude ratio as a function of nominal reduced velocity

**Table 2** Particulars of the flexible riser model

Item	Value
Diameter (mm)	28
Total length (m)	13.12
Mass ratio (mass/displaced mass of water)	3
Bending stiffness, EI ( $N\ m^2$ )	29.88
Range of Reynolds numbers	2500–25,000

11 and 12. This is due to the self-limiting nature of VIV. In these cases, the cross-flow vibrations are not dominant.

Figure 13 presents the RMS motion amplitude ratios (with respect to the riser diameter) in terms of the nominal reduced velocity and their comparison with the experimental data as well as those by Ma et al. [11]. The RMS amplitude ratio for each nominal reduced velocity was obtained using the displacement amplitudes in a duration of 150 s. It can be observed from Fig. 13 that the present method improved the predictions, especially at the low nominal reduced velocities.

#### 4.2 VIV of a flexible riser

The present numerical model was further validated by using the experimental results of a vertical flexible riser model in a stepped current [14]. The properties of the riser model are given in Table 2. The experimental set-up presented in Fig. 14 was taken from the work of Chaplin et al. [14].

Four cases were examined, which are corresponding to four current speeds and different initial top tensions as given in Table 3. All the simulations started from the static equilibrium positions with zero initial velocities. Hinged boundary conditions were applied to the ends of the riser in the simulations.

For each case, time series of the transverse motions at  $z = -0.25L$ ,  $z = -0.5L$  and  $z = -0.75L$  ( $z = 0$  is at the calm

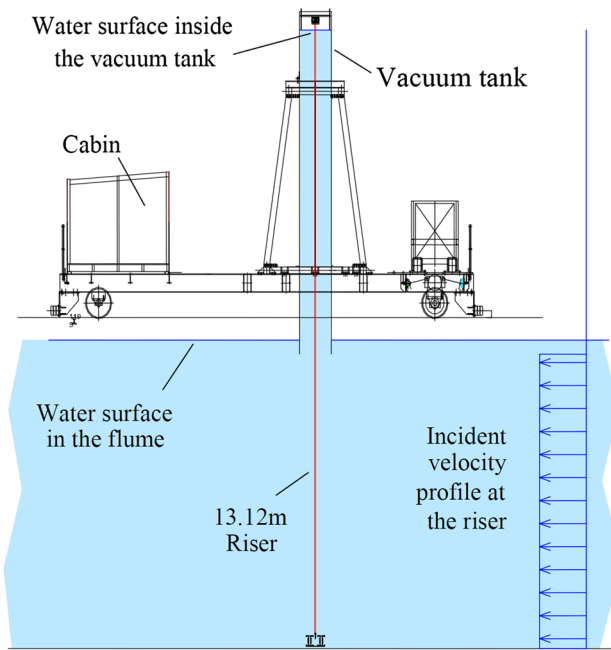


**Fig. 14** Set-up of VIV tests [14]

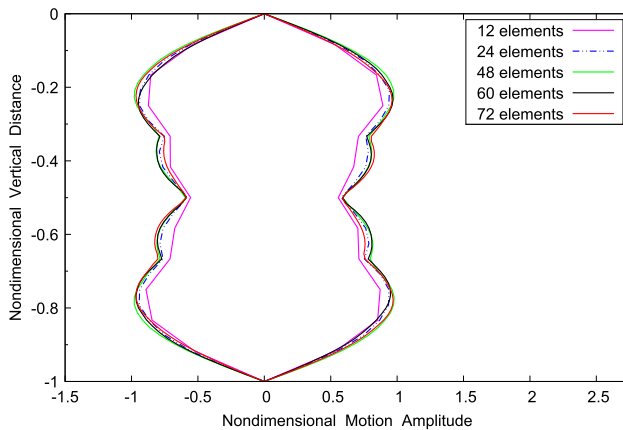


**Fig. 15** Convergence of predicted riser envelope to the number of elements

water surface and  $L$  is the riser length), the riser profiles at different time instants, and the cross-flow vibration envelopes are presented. The vibration envelopes were obtained by using the maximum and minimum displacements at each node over the entire simulation duration (300 s). Note that all the presented displacements were non-dimensionalized with respect to the diameter of the riser.

Convergence studies were carried out for the four cases by using various numbers of elements, 12, 24, 48, 60 and 72, and a number of time steps (0.0002, 0.0001 and 0.00005 s). As examples, Fig. 15 presents the convergence of the predicted envelope to the number of elements using the time step of 0.0001 s for the current velocity of 0.31 m/s. It can

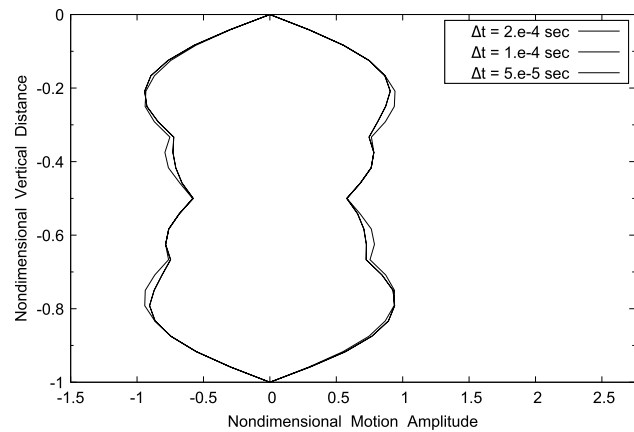


**Fig. 16** Convergence of predicted riser envelope to time step

**Table 3** Simulation scenarios for the flexible riser

Case no.	Current velocity $U$ (m/s)	Initial top tension (N)
1	0.16	405
3	0.31	457
6	0.60	670
9	0.95	1002

be observed that the solutions converge as the number of elements increased. Figure 16 shows the convergence of the predicted envelope for the same current velocity with respect to the time step using 24 elements. It can be seen that the numerical prediction is insensitive to the time step. In the following figures, all the results were based on 72 elements and the time step of 0.0001 s.

The predicted envelopes were compared to the experimental results (Chaplin et al. [14]) and the numerical solutions by SHEAR7, Norsk Hydro and Ma et al. [11]. Note that Norsk Hydro predicts VIV by coupling the computation of the hydrodynamic forces on 2-D planes using computational fluid dynamics (CFD) with a finite element structural code [15]. In the work of Ma et al. [11], all the results were obtained using 200 elements and a time step of 0.0025 s. The results by SHEAR7 and Norsk Hydro were taken from the work by Chaplin et al. [16].

#### 4.2.1 Case 1: $U = 0.16$ m/s

Figures 17, 18 and 19 present the time series of the displacements at the midpoint,  $z = -0.25L$ , and  $z = -0.75L$ , respectively. From these figures, it can be seen that the motions include different frequency components. The steady state

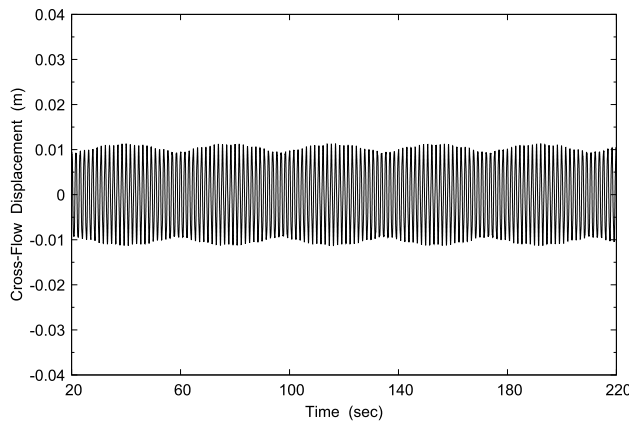


**Fig. 17** Time series of cross-flow motion at the midpoint for Case 1

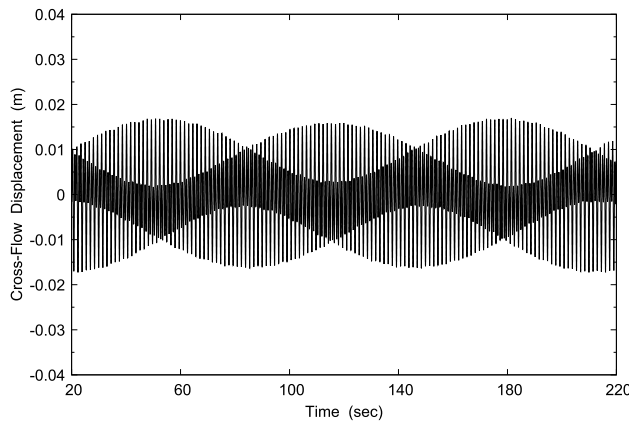


**Fig. 18** Time series of cross-flow motion at  $z = -0.25L$  for Case 1

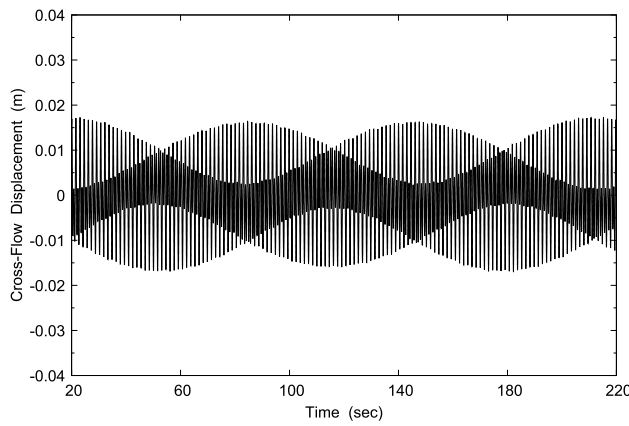


**Fig. 19** Time series of cross-flow motion at  $z = -0.75L$  for Case 1

was reached after a transient period. The corresponding riser profiles at different time instants are presented in Fig. 20.

The comparison of the envelope predicted by the present model, the experimental one and those by SHEAR7, Norsk

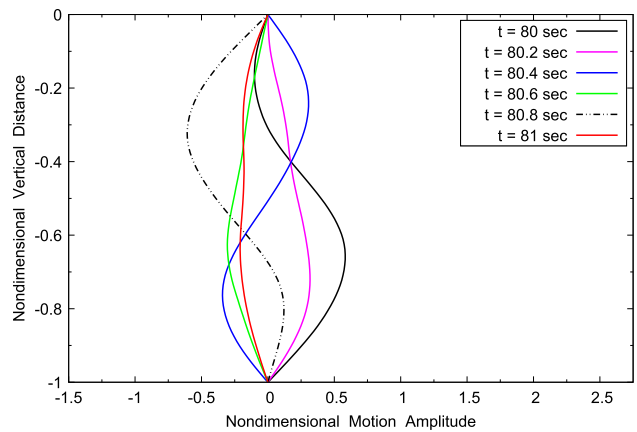


**Fig. 20** Riser profiles at different time instants for Case 1

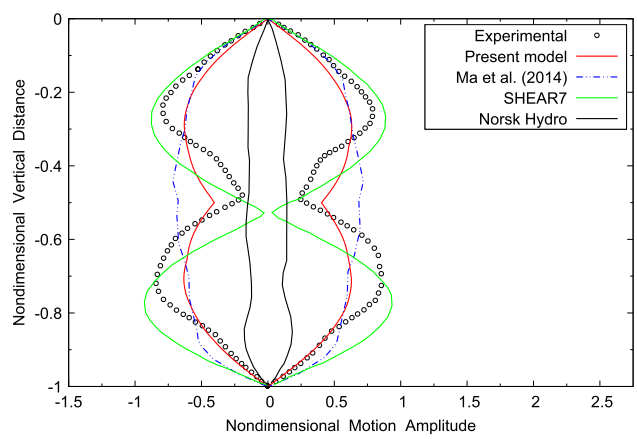


**Fig. 21** Comparison of cross-flow vibration envelope for Case 1

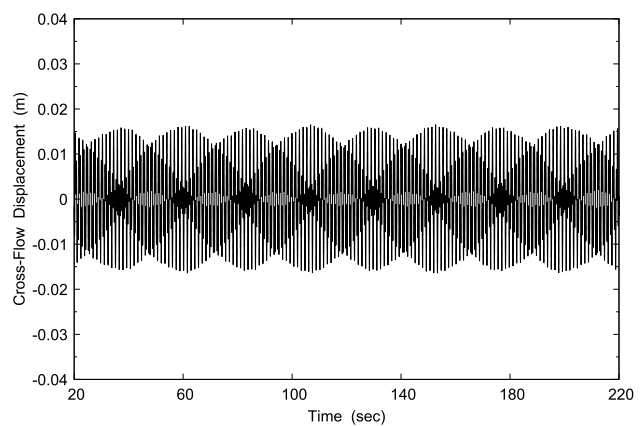


**Fig. 22** Time series of cross-flow motion at the midpoint for Case 3

Hydro and by Ma et al. [11] is presented in Fig. 21. The modal shapes were not well captured in the work by Ma et al. [11] and by Norsk Hydro. It can be shown that the

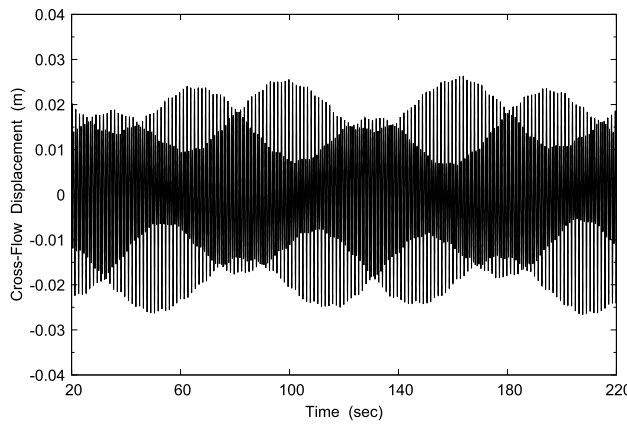


**Fig. 23** Time series of cross-flow motion at  $z = -0.25L$  for Case 3

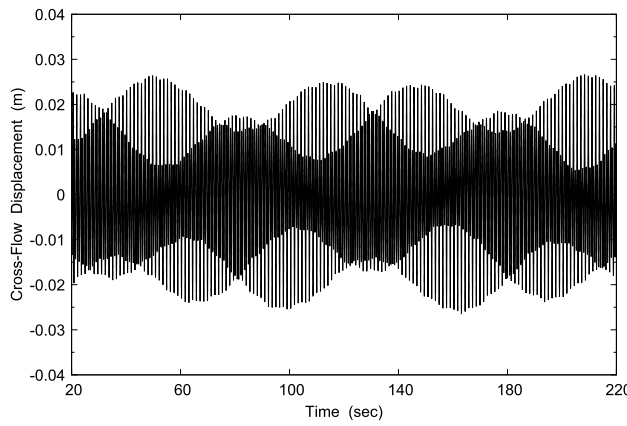


**Fig. 24** Time series of cross-flow motion at  $z = -0.75L$  for Case 3

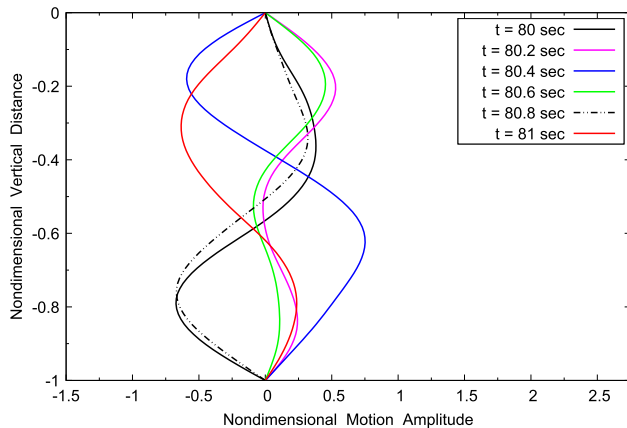


**Fig. 25** Riser profiles at different time instants for Case 3

present method led to an improvement in the prediction of modal shapes.

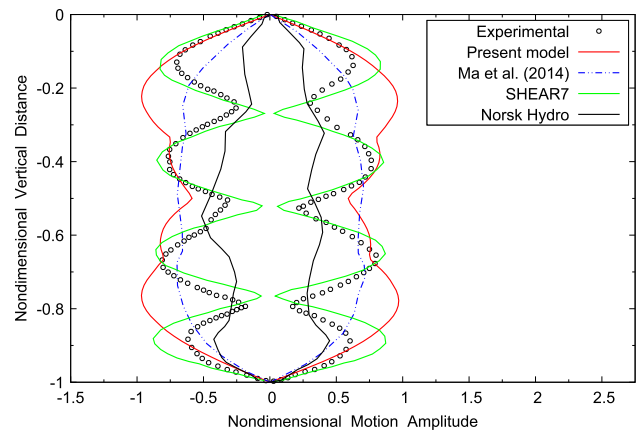


**Fig. 26** Comparison of cross-flow vibration envelope for Case 3

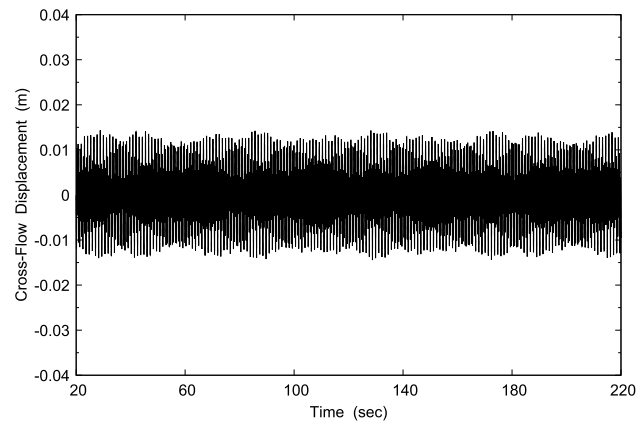


**Fig. 27** Time series of cross-flow motion at the midpoint for Case 6

#### 4.2.2 Case 3: $U = 0.31\text{ m/s}$

Figures 22, 23 and 24 present the time series of the displacements at the midpoint,  $z = -0.25L$ , and  $z = -0.75L$ , respectively. The riser profiles at different time instants are presented in Fig. 25.

The comparison of the predicted and experimental envelopes is given in Fig. 26. The present model over-predicted the responses. It is likely because the hydrodynamic database used in the computations corresponded to high Reynolds numbers, while the riser was subjected to a low Reynolds number in the tests.

#### 4.2.3 Case 6: $U = 0.6 \text{ m/s}$

Figures 27, 28 and 29 present the time series of the displacements at the midpoint,  $z = -0.25L$ , and  $z = -0.75L$ , respectively. Different frequency components can be observed in the time series. The steady state was reached after a transient

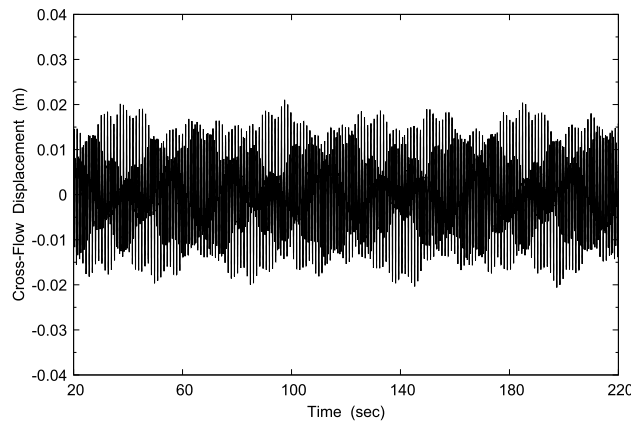


**Fig. 28** Time series of cross-flow motion at  $z = -0.25L$  for Case 6

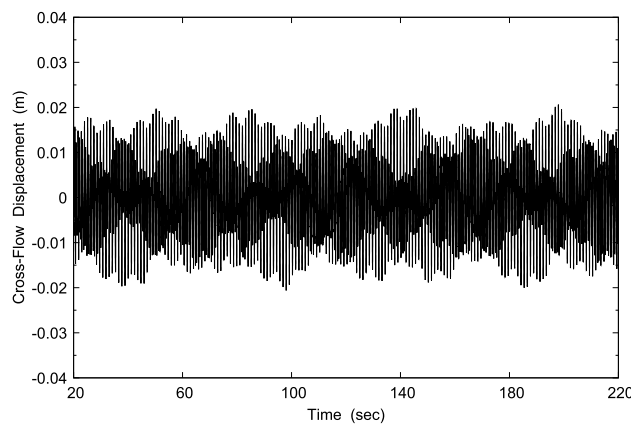


**Fig. 29** Time series of cross-flow motion at  $z = -0.75L$  for Case 6

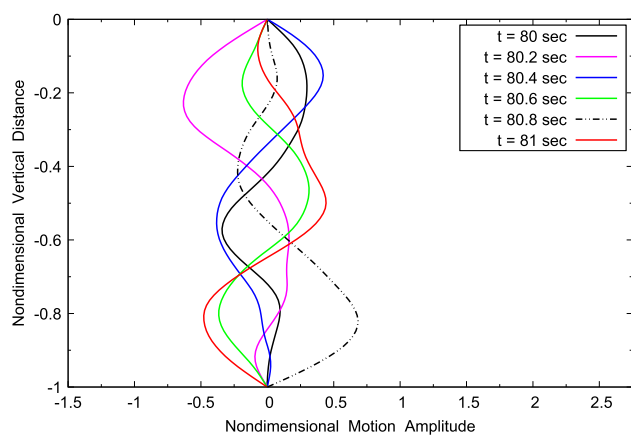


**Fig. 30** Riser profiles at different time instants for Case 6

period. The riser profiles at different time instants are presented in Fig. 30.

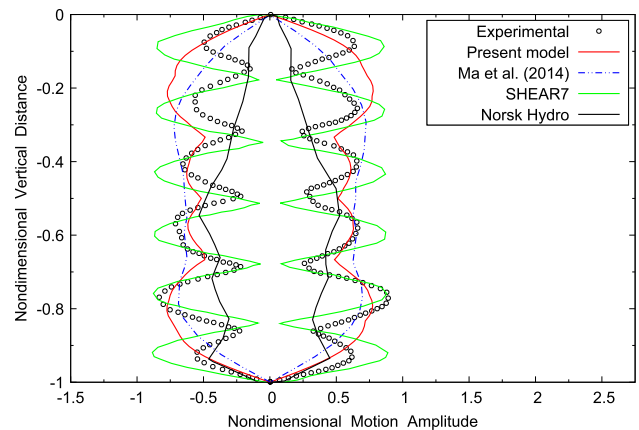


**Fig. 31** Comparison of cross-flow vibration envelope for Case 6

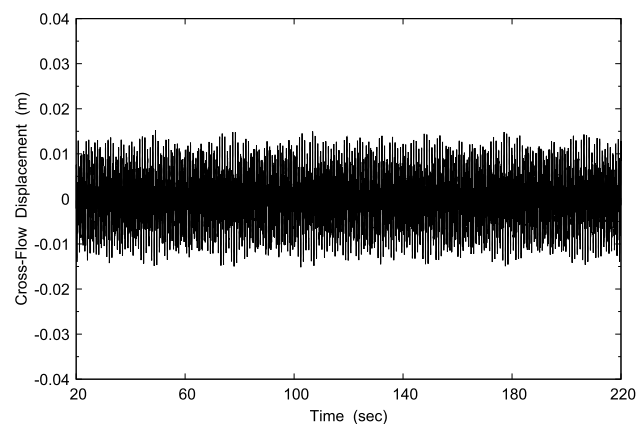


**Fig. 32** Time series of cross-flow motion at the midpoint for Case 9

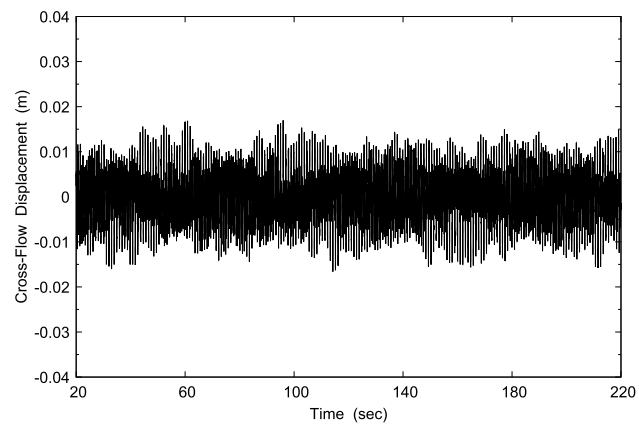


**Fig. 33** Time series of cross-flow motion at  $z = -0.25L$  for Case 9

The comparison of the envelopes with other results is given in Fig. 31. Similar observation to that in Case 3 can be obtained.

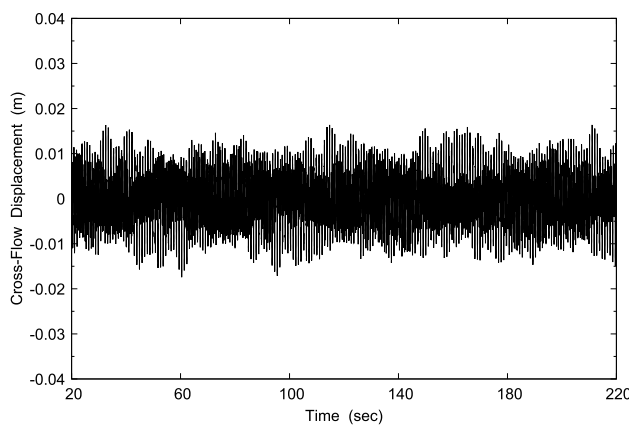


**Fig. 34** Time series of cross-flow motion at  $z = -0.75L$  for Case 9

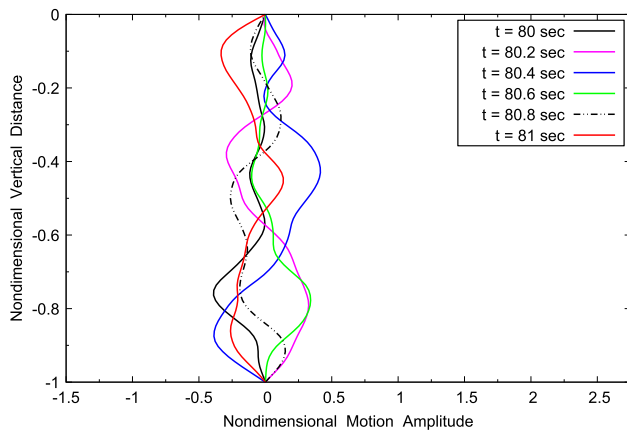


**Fig. 35** Riser profiles at different time instants for Case 9

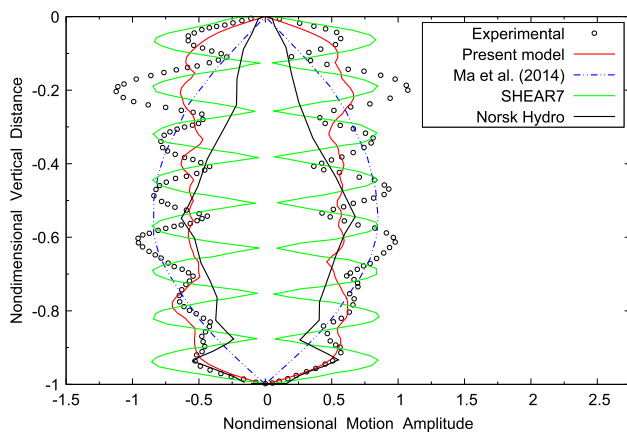


**Fig. 36** Comparison of cross-flow vibration envelope for Case 9

#### 4.2.4 Case 9: $U = 0.95 \text{ m/s}$

Time series of the riser displacements at the midpoint,  $z = -0.25L$  and  $z = -0.75L$  are presented in Figs. 32, 33, and 34, respectively. The riser profiles at different time instants are presented in Fig. 35.

Figure 36 presents the comparison of the experimental envelope and those by the present method, SHEAR7 and Norsk Hydro, as well as those by Ma et al. [11]. The proposed method by Ma et al. [11] was not able to capture the modal shapes. The present model shows improvement in modal prediction but with under-predicted values. This may be due to the issue associated with different Reynolds numbers as discussed earlier.

It should be noted that the experimental cross-flow deflections were obtained by the double integration of the strain gauge signals at 32 stations along the riser span. Although uncertainty analysis was not carried out in the work of Chaplin et al. [14], uncertainties in the measurements could contribute to the discrepancies between the experimental and numerical results. In addition, the top end of the riser was suspended from a spring system during the tests, while a hinged boundary condition at the top end was employed in numerical simulations. This could lead to the underestimation of displacements.

## 5 Conclusions

A time-domain model was further developed to predict the vortex-induced vibration (VIV) of marine risers. Using the zero up-crossing analysis of the cross-flow displacement, two state variables, i.e., amplitude ratio and reduced velocity, were obtained to interpolate the hydrodynamic coefficients from a database, which is based on forced oscillation tests of a full-scale riser segment at high Reynolds numbers. The forcing algorithm was then integrated into a global-coordinate-based finite element program to simulate the riser VIV in the time domain. Validation studies were carried out for a rigid riser in a uniform flow and a flexible riser in a stepped current. The predicted cross-flow motions were compared with the experimental data and the results by other numerical methods. In comparison with the earlier work in Ma et al. [11], the present method has improved the prediction of cross-flow displacements of the rigid riser and the envelopes of a flexible riser.

Further validation studies should be carried out on flexible risers at higher Reynolds numbers and the Reynolds effects need to be investigated. Moreover, the hydrodynamic database should include more data points in order to improve the accuracy of interpolations.

**Acknowledgements** This work was supported by the Natural Science and Engineering Research Council (NSERC) of Canada.

## References

1. M. Triantafyllou, G. Triantafyllou, Y. Tein, B. Ambrose, Pragmatic riser VIV analysis, in *Proceedings of Offshore Technology Conference* (1999)
2. C. Larsen, *Empirical VIV Models, Workshop on Vortex-Induced Vibrations (VIV) of Offshore Structures*. São Paulo, Brazil (2000)
3. M. Venugopal, Damping and response prediction of a flexible cylinder in a current, Ph.D. Thesis, Massachusetts Institute of Technology (1996)
4. R. Gopalkrishnan, Vortex-induced forces on oscillating bluff cylinders, Ph.D. Thesis, Massachusetts Institute of Technology (1993)
5. O. Oakley, D. Spencer, Deepstar high Reynolds number cylinder test program, in *Proceedings of Deep Offshore Technology Conference* (2004)
6. H. Lie, A time domain model for simulation of vortex induced vibrations on a cable, in *Flow-Induced Vibration*, pp. 455–466 (1995)
7. L. Finn, K. Lambrakos, J. Maher, Time domain prediction of riser VIV, in *Proceedings of the Fourth International Conference on Advances in Riser Technologies*, Aberdeen, Scotland (1999)
8. D. Sidarta, L. Finn, J. Maher, Time domain FEA for riser VIV analysis, in *Proceedings of 29th International Conference on Ocean, Offshore and Arctic Engineering* (2010)
9. M. Thorsen, S. Sævik, C. Larsen, A simplified method for time domain simulation of cross-flow vortex-induced vibrations. *J. Fluids Struct.* **49**, 135–148 (2014)
10. D. Spencer, H. Yin, W. Qiu, Development and verification of a time-domain viv simulation tool, in *Proceedings of the 3rd International Workshop on Applied Offshore Hydrodynamics*, Rio de Janeiro, Brazil (2007)
11. P. Ma, W. Qiu, D. Spencer, Numerical vortex-induced vibration prediction of marine risers in time-domain based on a forcing algorithm, *J. Offshore Mech. Arctic Eng.* **136**(3) (2014)
12. H. Yin, W. Qiu, Dynamic analysis of mooring line in the time domain, in *Proceedings of 8th Canadian Marine Hydromechanics and Structures Conference*, St. John's, Canada (2007)
13. D. Garrett, Dynamic analysis of slender rods. *J. Energy Resour. Technol.* **104**, 302–306 (1982)
14. J.R. Chaplin, P.W. Bearman, F.J. Huera Huarte, R.J. Pattenden, Laboratory measurements of vortex-induced vibrations of a vertical tension riser in a stepped current. *J. Fluids Struct.* **21**, 3–24 (2005)
15. K. Herfjord, S. Drange, T. Kvamsdal, Assessment of vortex-induced vibrations on deepwater risers by considering fluid–structure interaction. *J. Offshore Mech. Arctic Eng.* **121**, 207–212 (1999)
16. J.R. Chaplin, P.W. Bearman, Y. Cheng, E. Fontaine, J.M.R. Graham, K. Herfjord, F.J. Huera Huarte, M. Isherwood, K. Lambrakos, C.M. Larsen, J.R. Meneghini, G. Moe, R.J. Pattenden, M.S. Triantafyllou, R.H.J. Willden, Blind predictions of laboratory measurements of vortex-induced vibrations of a tension riser. *J. Fluids Struct.* **21**, 25–40 (2005)